



# Laboratory study of the electrical properties of Lutetian limestones in the 100 Hz to 10 MHz frequency range

Blaise Souffaché, Alain Tabbagh

## ► To cite this version:

Blaise Souffaché, Alain Tabbagh. Laboratory study of the electrical properties of Lutetian limestones in the 100 Hz to 10 MHz frequency range. *Near Surface Geophysics*, 2021, 19, pp.573 - 582. 10.1002/nsg.12167 . hal-03823577v2

**HAL Id: hal-03823577**

**<https://cnrs.hal.science/hal-03823577v2>**

Submitted on 21 Oct 2022

**HAL** is a multi-disciplinary open access archive for the deposit and dissemination of scientific research documents, whether they are published or not. The documents may come from teaching and research institutions in France or abroad, or from public or private research centers.

L'archive ouverte pluridisciplinaire **HAL**, est destinée au dépôt et à la diffusion de documents scientifiques de niveau recherche, publiés ou non, émanant des établissements d'enseignement et de recherche français ou étrangers, des laboratoires publics ou privés.

# Laboratory study of the electrical properties of Lutetian limestones in the 100 Hz to 10 MHz frequency range

Blaise Souffaché\* and Alain Tabbagh

Sorbonne Université, CNRS, EPHE, UMR7619, Métis, 4 place Jussieu, Paris, 75252, France

Received November 2020, revision accepted May 2021

## ABSTRACT

Lutetian limestones have been widely used in historical monuments within the Paris Basin during the course of the medieval and modern periods. Among the physical properties that can be used to assess the evolution of the limestones *in situ* in the buildings and their present health, the complex effective permittivity in the 10–100 kHz frequency range is easy to measure and reflects the internal structure of the stone along with the dependence on the water content. To improve our knowledge about this property, a laboratory study on four samples collected in the relevant quarries has been undertaken using measurements in the 100 Hz–10 MHz frequency range. Except close to zero water content, the observed results exhibit a quasi-absence of variation of the real effective permittivity with the water content. The frequency variation fits fairly well with a model taking into account a Jonscher's decrease, a direct current conductivity, a high-frequency dielectric permittivity and losses, and a relaxation phenomenon. When fitted by a Cole–Cole model, the magnitude of the corresponding relative permittivity change always stays close to 30, but the time constant varies from 1.0  $\mu$ s to 0.1  $\mu$ s as the water content increases.

**Key words:** Archaeogeophysics, Conductivity, Dielectric properties, Non-destructive.

## INTRODUCTION

Carbonate rocks account for an important portion of the sedimentary rocks present in the surficial layers of the Earth. They are often sufficiently porous and permeable to play a significant part in the processes of transfer and storage of groundwater or hydrocarbons; moreover, they have also played a determining role as materials used for construction since the beginnings of human society settlements. As for other sedimentary rocks, there exist numerous publications dealing with electrical resistivity/conductivity as well as with their induced polarization at frequencies lower than 100 Hz (Keller and Frischknecht, 1966, Olhoeft, 1985, Kenma *et al.*, 2012); for higher ‘intermediate’ frequencies, see Knight and Nur (1987).

In the perspective of civil engineering applications and for construction, sedimentary rocks deserve special attention

because builders have to be able to evaluate the interest of their extraction *in situ* and then to monitor over time their alteration in place in constructions. Restorers and building archaeologists have to assess their present health (Rozenbaum *et al.*, 2007) and also intend to identify the choices that could have been those of the builders of ancient monuments (Souffaché *et al.*, 2016). Good knowledge of the physical properties of these natural sedimentary materials is essential to achieve correct interpretations of the geophysical or non-destructive tests whatever investigation technique is used. In the present study, the electrical properties are considered. They are expressed in terms of complex effective permittivity, where the real component corresponds to the global electrical polarization and the imaginary component comprises both the direct current conductivity and dielectric losses.

This experimental study is limited to the Lutetian limestones of the Paris Basin, the use of which as masonry stones has been very important in medieval and modern periods in

---

\*Email: blaise.souffache@upmc.fr

spite of lateral variations of facies (Fronteau *et al.*, 2010). A large number of quarries were operated on the whole Basin with numerous different techniques (Devos *et al.*, 2010). The major component of these limestones is calcite, with minor contents of quartz sand and clay minerals. These latter play an important role in the response to the application of an electric field due to their high specific surface with ionic double layer (Stern and diffuse layers) surrounding the clay particles (Leroy and Revil, 2009). The *in situ* measurements on ancient monuments (Souffaché *et al.*, 2016) using a decimetric sized instrument showed over two different depth of investigation (approximately 10 cm and 20 cm) significant variations of both the real and imaginary components of the effective permittivity over the whole volume of masonry stones belonging to the facings. It is worth noting that in the older monuments, i.e. having exceeded a half-century of existence, the water content of the stone is constant beyond two to three centimetres whatever the weather conditions (Sass and Viles, 2010). Where constructions are protected by roofs, weather fluctuations only lead to pellicle variations of the stone water content, conversely a significant water content would evidence a lack of protection. Moreover, to get a global overview regarding the electrical properties of these stones and due to the huge impact of the water content on electrical properties of rocks and soils in general, it is inescapable to also investigate its exact role.

The following experimental study is made at laboratory temperature ( $\sim 20^\circ\text{C}$ ) and does not consider the effect of the temperature, which *in situ* may vary from  $-10^\circ\text{C}$  to  $35^\circ\text{C}$  at the masonry stone surface and may affect the ion mobility. Our work investigates the role of the liquid water content before paying particular attention to the frequency variations of the electrical properties of the four considered samples.

## MATERIALS AND METHODS

### Samples

Our study is limited to limestones used in the Paris region for the construction of monuments. The materials studied in the laboratory are extracted from the same beds as those present in the monuments. They are Lutetian limestones coming from the Saint Pierre Aigle (Aisne), Château Landon (Seine et Marne) and the Saint Maximin (Oise) (two samples referenced by 3B and 3E) quarries in the Paris Basin. The first two samples correspond to ‘strong’ masonry stones called ‘Liais’ by quarry workers, the two others to ‘light’ masonry stones called ‘Vergelé’ by quarry workers.

Their mineralogical composition is only prone to weak variations of facies with regard to the three major phases present in limestones: calcite 92% to 97%; quartz (silt); and phyllosilicates (clay) a few percentages (Blondeau *et al.*, 1980). The ‘Vergelé’ samples correspond to the higher calcite content; their clay content is thus around 3%. However, there may be a difference in nature of the argillaceous phase between extraction sites; the clay can be pure illite, while smectite as well as interlayered clay add themselves in variable proportion to illite in another site. The difference between these two types of clay lies in the interfoliar cations: potassium for the illite, calcium and sodium for the smectite.

The samples, approximately weighing 1 kg, were first saturated by immersion in tap water of  $\sigma_w = 0.05 \pm 0.002 \text{ Sm}^{-1}$  conductivity during 48 h. Their open porosity, varying from 6% to 40%, led to the absorption of water, with amounts ranging from 20 g to  $\sim 180$  g. Effective permittivity measurements were made during free drying, each data acquisition being separated from the preceding by a weight loss of approximately 5 g. Last acquisitions at low water content were made after drying in an oven at  $50^\circ\text{C}$  for 24 hours.

### Measuring instrument

The measurement of the complex effective permittivity,  $\varepsilon$ , was carried out by means of a capacitive cell in which the limestone block of  $160 \times 160 \times 19 \text{ mm}^3$  volume was placed between two metal plates and excited by an electric field with frequencies varying between 100 Hz and 10 MHz. Both the applied signal and the response are performed by a PSM 1735 vector multi-metre (Phase Sensitive Meter, NumetricQ Ltd) (Fig. 1).

The instrument was first tested with moist clean sand, to assess its ability to follow low values and to compare the results with published calibration curves. We chose Fontainebleau sand and made measurements during free drying at regular intervals of time. The results fit with the high-frequency law (Topp *et al.*, 1980) in good agreement with the role played in permittivity value by the free water molecule rotation ( $\sim 80$ ).

### Modelling

After analysing the frequency variation of the samples, an empirical model was derived to describe the different behaviours successively observed. The general model fitting the data (see figures below) comprises five terms (where  $\omega$  is the angular frequency). The first corresponds to a Jonscher’s decrease (Jonscher, 1977) of the real part from the value  $\varepsilon_j$ , – the effective

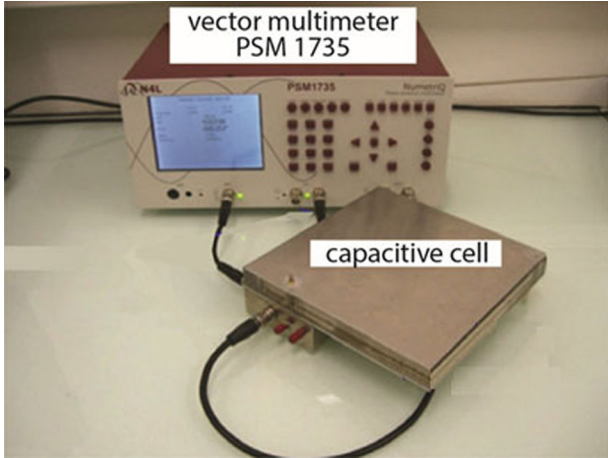


**Figure 1** Instrumentation: capacitive cell and PSM vector multi-meter. The limestone blocks are  $160 \times 160 \times 19 \text{ mm}^3$  sized.

permittivity that must be added at 100 Hz (corresponding angular frequency  $\omega_j$ ) – to fit the datum. This decrease is characterized by the negative exponent,  $n$ . This global behaviour does not result from an identified physical phenomenon, but rather a number of possible different phenomena and of their interactions. The second corresponds to the contribution of the DC conductivity,  $\sigma$ , to the imaginary part. The third corresponds to a relaxation, which is described by the Cole–Cole empirical expression (Cole and Cole, 1941); in this expression, the relative permittivity step  $\Delta\epsilon$ , the central time constant,  $\tau$ , and the exponent,  $c$ , which characterizes the relaxation distribution around  $\tau$  (there may exist several relaxations), intervene. The fourth and the fifth correspond to high-frequency relative real,  $\epsilon'_{HF}$ , and imaginary,  $\epsilon''_{HF}$ , parts. The complete expression of the effective relative permittivity is thus written:

$$\epsilon(\omega) = \epsilon_j \left( \frac{\omega}{\omega_j} \right)^n - i \frac{\sigma}{\omega \epsilon_0} + \frac{\Delta\epsilon}{1 + (i\omega\tau)^c} + \epsilon'_{HF}(\omega) - i\epsilon''_{HF}(\omega). \quad (1)$$

The fit between the model of effective permittivity and the measured permittivity values is controlled by the error expression,  $R$ :

$$R = \frac{1}{N} \sum_{i=1}^N \frac{|\epsilon_i^{\text{obs}} - \epsilon_i^{\text{Th}}|}{\epsilon_i^{\text{obs}}}, \quad (2)$$

where  $\epsilon_i^{\text{obs}}$  is the observed complex effective permittivity,  $\epsilon_i^{\text{Th}}$  the modelled value, and  $N$  the number of frequency measurements.

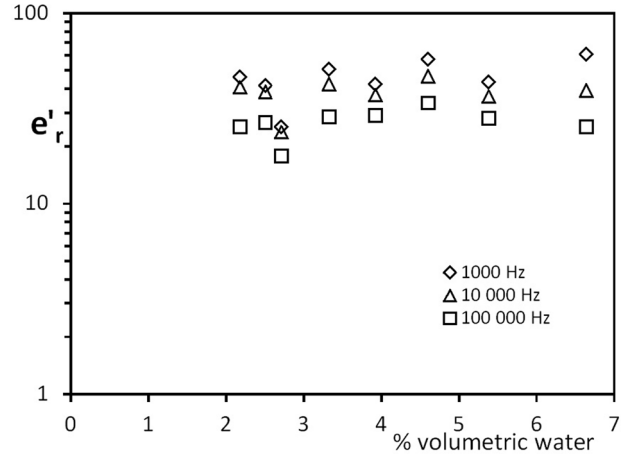


**Figure 2** Real part of the effective permittivity of the Château Landon sample as a function of water content at 1, 10 and 100 kHz.

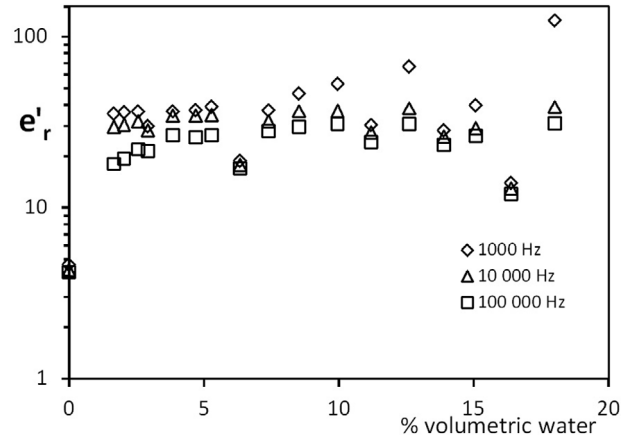


**Figure 3** Real part of the effective permittivity of the Saint Pierre Aigle sample as a function of water content at 1, 10 and 100 kHz.

## INFLUENCE OF THE WATER CONTENT AT FIXED FREQUENCIES

It is common, when considering the electrical/electromagnetic properties of rocks, to first question the role of the volumetric water content,  $\theta$ . The first characteristic that can be derived from this parameter is the porosity,  $\phi$ , deduced from the value at saturation. As can be expected for the geological contexts, Saint Maximin samples exhibit high porosities, greater for 3B (0.411) than for 3E (0.331); Saint Pierre–Aigle samples have a medium porosity (0.189), and Château Landon the lowest (0.0664).

The variations of the real part of the effective permittivity are presented in Figures 2–5. For the Château Landon and Saint Pierre Aigle samples with lower porosities, the scattering is significant, but it must be observed that, while gently increasing at 1 kHz, the values are quasi-constant above  $\theta =$

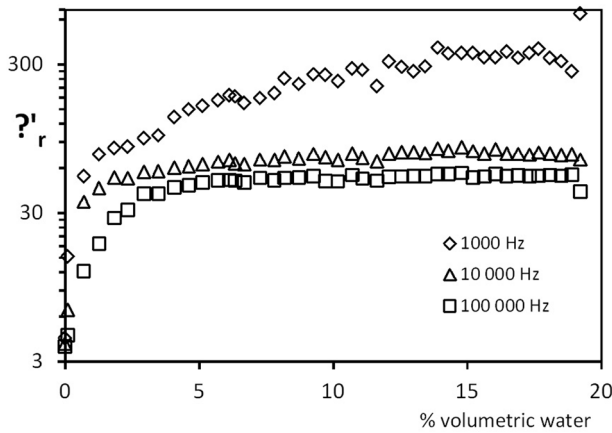


Figure 4 Real part of the effective permittivity of the Saint Maximin 3B sample as a function of water content at 1, 10 and 100 kHz.

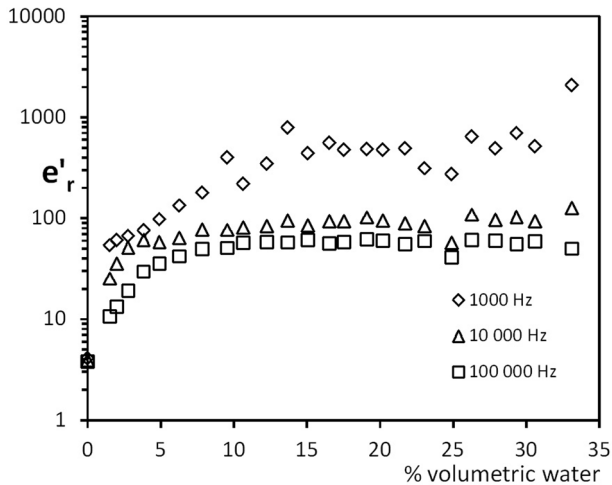


Figure 5 Real part of the effective permittivity of the Saint Maximin 3E sample as a function of water content at 1, 10 and 100 kHz.

0.02 for 10 kHz and 100 kHz. For Saint Maximin samples with higher porosities, the increase is sensible until  $\theta = 0.09$ . Contrary to the 1 kHz increase, the 10 kHz and 100 kHz variations are very small. As detailed below, this stability results from a compensation effect between higher  $\varepsilon_J$  values and more negative Jonscher's exponent,  $n$ .

## RESULTS OF THE FREQUENCY-DEPENDENCE MODELLING

### Château Landon

In this very low porosity sample,  $\varphi = 0.0664$ , the volumetric water content range of variation is limited. The frequency behaviour of the effective relative permittivity for different  $\theta$  val-

ues is illustrated in Figure 6, where the measured values are in black dots, the real part of the fitting curve in red and its imaginary part in blue. The main observable feature is the presence of a relaxation phenomenon that moves to higher frequency as the water content increases (Fig. 10). The conductivity effect is observable from 0.0333 water content, but not at 0.0218 due to the limits of the instrument. The slopes fitted by a Jonscher's expression also manifest themselves at upper water contents. The different modelling parameters are given in Table 1 for the whole water content range that is feasible with this sample. As the water content increases, the Jonscher's exponent,  $n$ , decreases from  $-0.1$  to  $-0.5$ ,  $\varepsilon_J$ ,  $\sigma$  and  $\varepsilon'_{HF}$  all increase,  $\Delta\varepsilon$  is scattered around 22, but slightly decreasing,  $c$  lies in the  $[0.74, 0.88]$  interval, and  $\tau$  decreases. The  $\tau$  variation is illustrated in Figure 10 together with the other samples to facilitate comparison. It can be approximated by a linear log-log variation and then follows a law of power with a  $-1.12$  rate and with a resulting Pearson's correlation coefficient of 0.89 (based on six observations).

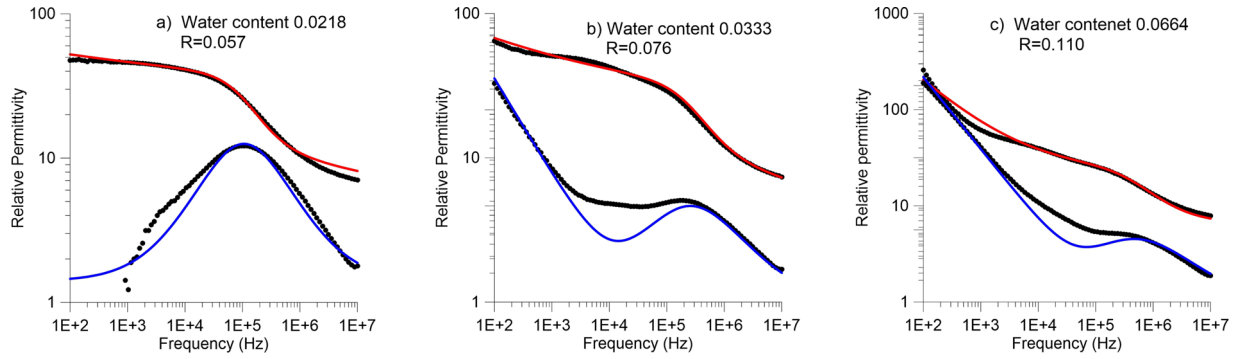
### Saint Pierre Aigle

Figure 7 demonstrates the measured and modelled results of the real and imaginary relative electric permittivity for four different water content levels (measurements in black dots, curve fitting the real part in red, curve fitting the imaginary part in blue) of the relative effective permittivity. As before, for the lower value of  $\theta$ , the conductivity influence on the imaginary part cannot be observed. For higher values, it generates a linear decrease of the imaginary part, but of significantly greater magnitude than the real part in the lower portion of the frequency range. Here, again, the Jonscher's decrease, not observable for lower  $\theta$  values, exhibits increasing presence at larger water contents. For this sample, the existence of a distinct relaxation phenomenon again is the major feature of the curves.

Table 2 gives the values of the different model parameters along the widest water content range possible for this sample. The Jonscher's exponent decreases from 0 to  $-1$ ,  $\varepsilon_J$ ,  $\sigma$  and  $\varepsilon'_{HF}$  all increase,  $\Delta\varepsilon$  slightly decreases,  $c$  lies in the  $[0.62, 0.88]$  interval and  $\tau$  decreases. The  $\tau$  variation, illustrated in Figure 10, follows a law of power with a  $-1.26$  rate and with a resulting Pearson's correlation coefficient of 0.99 (from 11 observations).

### Saint Maximin sample 3B

This first sample of Saint Maximin presents the greatest porosity,  $\varphi = 0.411$ , the extent in water content variations is thus



**Figure 6** Château Landon sample: frequency dependence of the relative permittivity for different volumetric water contents. Measured data in black dots, theoretical curves in red for the real component and in blue for the imaginary component. R is the residual relative error.

**Table 1** Numerical values of the model parameters obtained by fitting with the whole water content range for the Château Landon sample

$\theta$	$n$	$\varepsilon_J$	$\sigma$ ( $\mu\text{S/m}$ )	$\varepsilon'_{HF}$	$\varepsilon''_{HF}$	$\Delta\varepsilon$	$c$	$\tau$ ( $\mu\text{s}$ )
0.0218	-0.135	22	0	3.40	1.4	27	0.88	1.50
0.0271	-0.18	14	0	3.60	0.7	14.5	0.74	0.65
0.0333	-0.22	41	1.17	3.75	1.0	23	0.84	0.61
0.0461	-0.25	50	0.48	3.9	1.3	27	0.80	0.49
0.0539	-0.25	42	0.93	4.2	1.0	22	0.75	0.48
0.0664	-0.54	180	7.3	6.3	0.9	18	0.78	0.31

**Table 2** Numerical values of the model parameters obtained by fitting with the whole water content range for the Saint Pierre Aigle sample

$\theta$	$n$	$\varepsilon_J$	$\sigma$ ( $\mu\text{S/m}$ )	$\varepsilon'_{HF}$	$\varepsilon''_{HF}$	$\Delta\varepsilon$	$c$	$\tau$ ( $\mu\text{s}$ )
0.0167	0	1.0	0	3.22	0.3	30	0.62	1.75
0.0292	0	2.0	0	3.42	0.3	25	0.70	0.82
0.0384	-0.12	16	0.1	4.0	1.8	20	0.86	0.58
0.0469	-0.15	15	0.17	3.6	0.3	24	0.80	0.54
0.0582	-0.30	29	0.54	5.15	1.3	20	0.78	0.50
0.0740	-0.40	27	0.62	7.10	1.32	20.5	0.85	0.27
0.0853	-0.79	85	3.9	4.8	0.4	29	0.69	0.26
0.0995	-0.81	241	9.7	3.9	0.3	28	0.68	0.162
0.126	-0.88	438	15.0	7.1	1.2	22	0.79	0.12
0.151	-0.71	167	42.0	5.9	0.3	19	0.76	0.085
0.180	-0.944	1150	45.0	10.2	1.2	18.2	0.88	0.12

large and the permittivity reaches very high values as illustrated in Figure 8. The numerical values of the modelling parameters are presented in Table 3. With this sample, it has been possible to obtain a very low water content, where the frequency variation can be interpreted as simple decrease following a  $\tau = 3.6$  ms relaxation (the corresponding frequency, 44 Hz, lies outside the measurement interval). For the other values, one clearly observes the conductivity influence on the imaginary part. The Jonscher's exponent decreases from  $-0.72$  to  $-1.02$ ,  $\varepsilon_J$  exhibits a maximum at  $\theta = 0.279$ ,  $\sigma$  reaches a plateau for the higher water contents,  $\varepsilon'_{HF}$  regularly

increases,  $\Delta\varepsilon$  slightly decreases,  $c$  lies in the  $[0.76, 1]$  interval and  $\tau$  regularly decreases. The  $\tau$  variation is illustrated in Figure 10; contrary to the preceding samples, the curve is not approximately linear, but incurved for higher water contents.

### Saint Maximin sample 3E

This second sample of the same quarry has a lesser porosity,  $\varphi = 0.331$ , and its behaviour is somewhat different as illustrated in Figure 9 and Table 4. The Jonscher's exponent



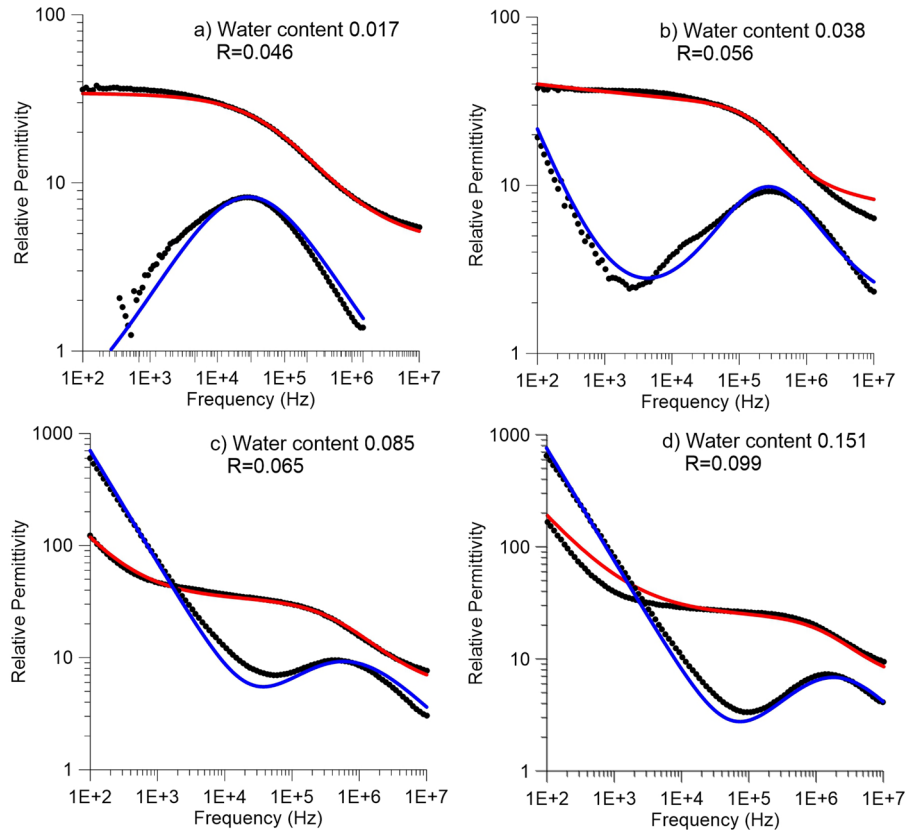


**Figure 7** Saint Pierre Aigle sample: frequency dependence of the relative permittivity for different volumetric water contents. Measured data in black dots, theoretical curves in red for the real component and in blue for the imaginary component.  $R$  is the residual relative error.

**Table 3** Numerical values of the model parameters obtained by fitting with the whole water content range for Saint Maximin 3B

$\theta$	$n$	$\varepsilon_I$	$\sigma$ ( $\mu\text{S/m}$ )	$\varepsilon'_{HF}$	$\varepsilon''_{HF}$	$\Delta\varepsilon$	$c$	$\tau$ ( $\mu\text{s}$ )
0.0017	0	0	0	3.2	0.1	180	0.66	3600
0.0222	-0.72	219	3.8	4.15	0.	30	0.76	1.6
0.0414	-0.85	280	5.2	6.1	0.75	38	0.85	0.85
0.0523	-0.65	300	5.6	5.4	0.80	37	0.82	0.485
0.0732	-0.87	750	17.2	5.0	0.2	40	0.79	0.32
0.117	-0.85	1000	26.	8.2	1.0	38	0.89	0.21
0.165	-0.90	1500	31.	11.0	2.5	37	0.95	0.185
0.207	-0.89	2000	44.	11.0	2.5	38	0.89	0.18
0.279	-0.96	3100	69.	15.	3.5	37	0.92	0.135
0.330	-1.02	2800	63.	18.	2.0	35	0.97	0.135
0.402	-0.97	2300	61.	22.	2.0	30	1.0	0.13

exhibits a larger interval,  $[-0.14, -1.25]$ , the  $\varepsilon_I$  and  $\sigma$  values reach greater values,  $c$  and  $\tau$  are comparable, but  $\Delta\varepsilon$  is slightly higher. As for the other Saint Maximin sample, the  $\tau$  variation (Fig. 10) is incurved and tends to stabilize around  $0.1 \mu\text{s}$  for the higher water contents.

## DISCUSSION

In the measured frequency range, the electrical and electromagnetic properties cannot be deduced from simple mixing laws based on the constituent high-frequency permittivity; 2.2 for calcite (crystal polarization) and 80 for water (rotation of

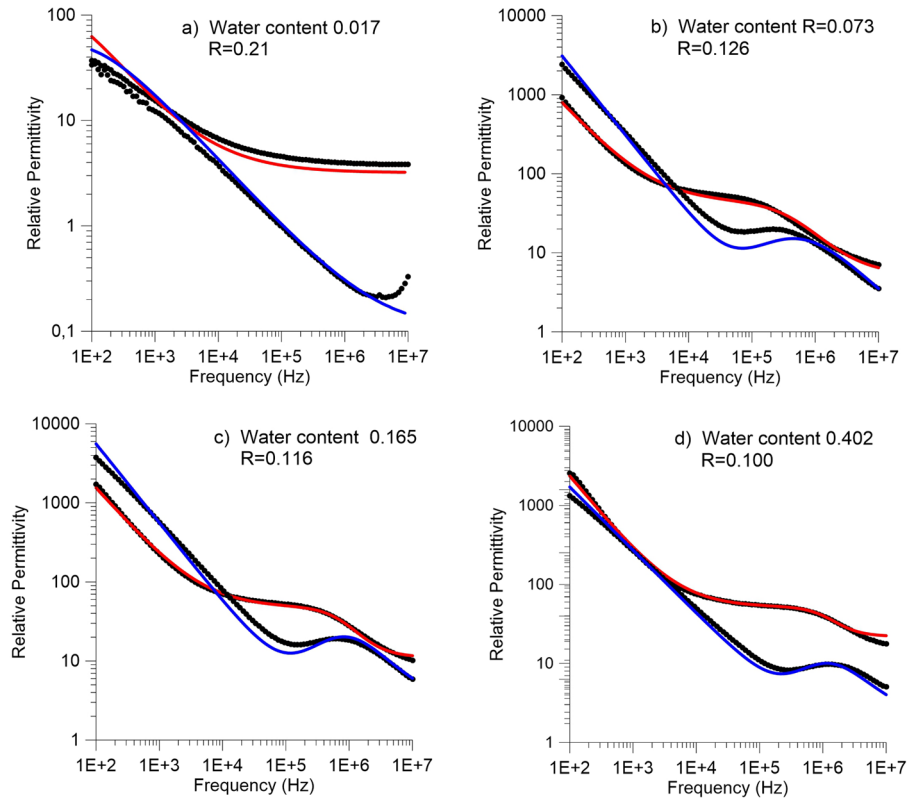


**Figure 8** Saint Maximin 3B sample: frequency dependence of the relative permittivity for different volumetric water contents. Measured data in black dots, theoretical curves in red for the real component and in blue for the imaginary component. R is the residual relative error.

**Table 4** Numerical values of the model parameters obtained by fitting with the whole water content range for Saint Maximin 3E

$\theta$	$n$	$\varepsilon_J$	$\sigma$ ( $\mu\text{S/m}$ )	$\varepsilon'_{HF}$	$\varepsilon''_{HF}$	$\Delta\varepsilon$	$c$	$\tau$ ( $\mu\text{s}$ )
0.015	-0.14	11	0	2.9	1.1	54	0.70	33.0
0.0278	-0.23	37	0.39	3.2	1.3	44	0.87	4.1
0.0491	-0.85	460	15.0	6.1	0.95	43	0.84	0.92
0.0783	-0.80	960	23.5	6.9	2.0	44	0.87	0.48
0.107	-0.87	1500	34.0	6.4	2.2	48	0.79	0.32
0.151	-0.97	4000	110.	7.7	1.9	52	0.82	0.19
0.191	-0.94	4000	106.	8.3	2.1	53	0.81	0.17
0.331	-1.25	34,000	1130.	14.5	2.0	35	0.80	0.10

free molecules). The arrangement and shapes of the grains, the pore networks, and the presence of clay platelets generate complex polarization phenomena. High permittivity values have theoretically (Tabbagh *et al.*, 2009) been modelled, but laboratory experiments are required to identify the phenomena acting in a given frequency range and to be able to interpret *in situ* measurements. One first observed strong changes of the permittivity values when the volumetric water content increases from 0.00 to 0.02 (for low porosity samples) or 0.08

(for high porosity samples), followed by limited variations. In monuments, masonry stones are protected by a roof and their volumetric water content, which is stable in relation to the average air humidity, stays in the 0.05–0.06 interval whatever the weather conditions. An increase of water content would indicate a degradation of the stones observable with the imaginary part (conductivity increase). In good conditions, one can expect that the impact of moisture change on the real part of the effective permittivity will be limited, whereas the structural



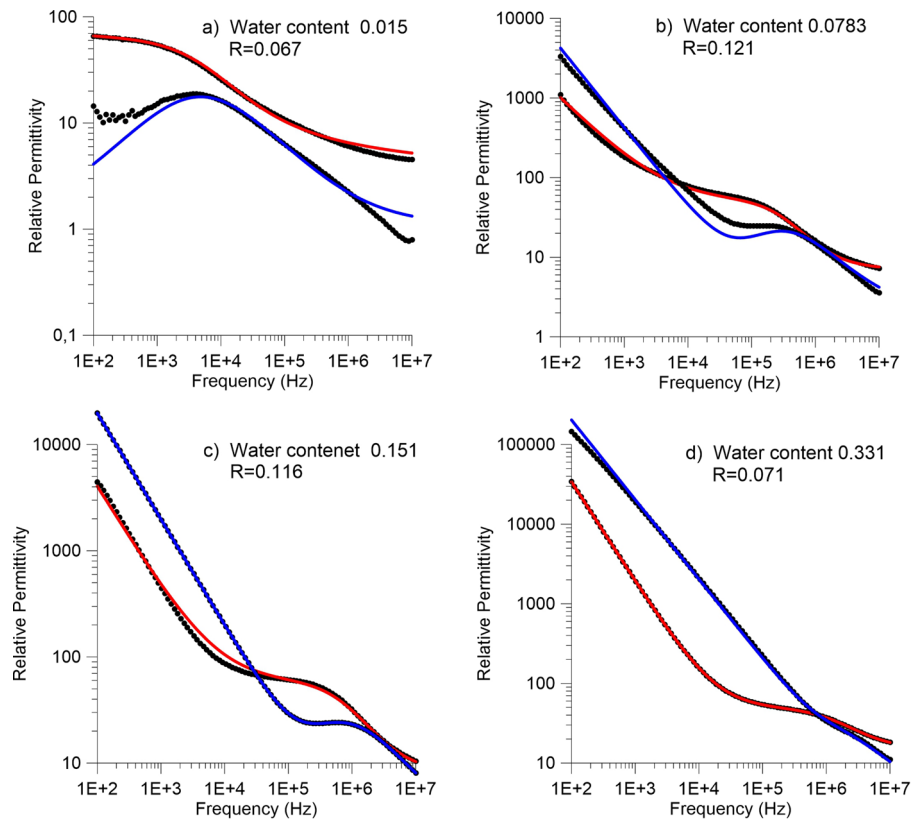


**Figure 9** Saint Maximin 3E sample: frequency dependence of the relative permittivity for different volumetric water contents. Measured data in black dots, theoretical curves in red for the real component and in blue for the imaginary component. R is the residual relative error.

characteristics of the solid grains nature and arrangement will play a more significant role and make the identification of masonry stone and facies changes quite easy.

Above c. 0.02 water content, the main characteristics of the frequency dependence of the complex effective permittivity are: (1) a global decrease against the frequency; and (2) the presence of a relaxation phenomenon. As expected, the decrease of the imaginary part is inversely proportional to the direct current conductivity value. The decrease of the real part can be described by a Jonscher's law that corresponds to a wide distribution of small relaxation phenomena. For all the samples the easily identifiable relaxation corresponds to time constants varying from  $1.0 \mu\text{s}$  to  $0.1 \mu\text{s}$  as the water content increases. This relaxation exists for very small water content, and the corresponding permittivity step,  $\Delta\epsilon$ , does not significantly change with the water content. Consequently, these two characteristics must probably be related to the presence of the electrical double layer (EDL) at the surface of clay platelets. The surficial ion quantity does not change, but in the absence of free water, with bounded water only, their displacement is slow, and as the free water content increases, their displace-

ment is facilitated. For this relaxation, the underlying process would then be the EDL polarization.

All these experimental data will be incorporated into to the general classification of the polarization phenomena (Kemna *et al.*, 2012; Loewer *et al.*, 2017; Niu *et al.*, 2020). However, this will be a difficult task, as the Jonscher's type decreases of the real parts with frequency correspond to large distributions of time constants and possibly to different polarization processes. Interestingly, it can be described by only two empirical parameters,  $\epsilon_j$  and  $n$ , the contradictory effect of which explains at fixed frequency the observed limited dependence on the water content.

## CONCLUSION

As regards the measuring point of view, the present experimental study first confirms that in the considered frequency range, the real part of the permittivity can be high, far higher than the one observed in the high-frequency ground-penetrating radar range. It can override the conductivity response expressed by the imaginary part and both components must be

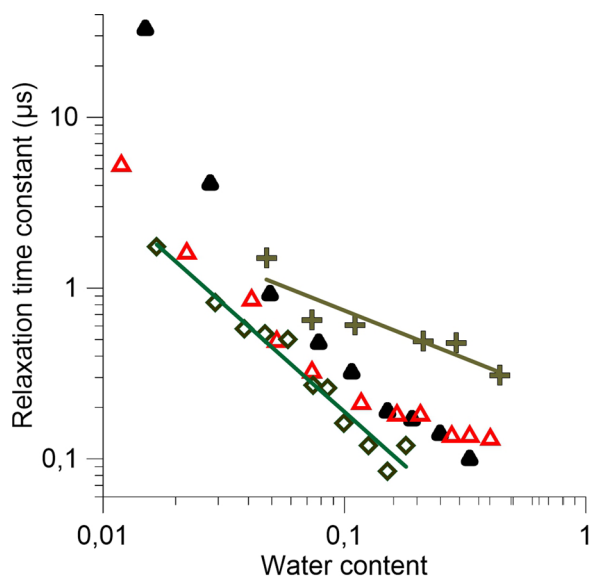


Figure 10 Four sample relationships between the relaxation time constant and the volumetric water content: for Château Landon (brown crosses) the power law slope is  $-1.12$ , for Saint Pierre Aigle sample (green diamonds) the power law slope is  $-1.28$ , for Saint Maximin 3B (red triangles) and 3E (black triangles) samples, the variations show a curvature and do not fit with a power law.


taken into account when measuring. This observation agrees well with the publications dealing with the 'intermediate' frequency range (Tabbagh *et al.*, 2021).

Concerning the stones themselves, we lack any comparison with other types of sedimentary and not sedimentary rocks, but the attribution to the clay fraction of the relaxation observed for these Lutetian limestones is proposed. A greater panel of experiments with deeper characterization remains now to be undertaken in order to better assess this hypothesis.

## ACKNOWLEDGEMENTS

The work was achieved with the contribution of Métis (UMR7619, Sorbonne Université) funds. In-kind contribution for stone characterization was provided by Dr Jean-Pierre Gély (Université Paris 1 Panthéon-Sorbonne). We warmly thank the Associate Editor and the two reviewers for their constructive criticism and suggestions.

## ORCID

Blaise Souffaché  <https://orcid.org/0000-0003-1607-8956>

Alain Tabbagh  <https://orcid.org/0000-0001-7858-8359>

## REFERENCES

- Blondeau, A., Cavelier, C., Labourguigne, J., Mégnién, C. and Mégnién, F. (1980) Eocène moyen. *Synthèse géologique du bassin de Paris*, mémoire BRGM n°101, chapitre 12, p. 374.
- Cole, K.S. and Cole, R.H. (1941) Dispersion and absorption in dielectrics 1. Alternating current characteristics. *Journal of Chemical Physics*, 9, 341–351.
- Devos, A., Fronteau, G., Lejeune, O., Sosson, C., Chopin, E. and Barbin, V. (2010) Influence of geomorphological constraints and exploitation techniques on stone quarry spatial organization. Example of Lutetian underground quarries in Reims, Laon and Soisson areas. *Engineering Geology*, 115, 268–275.
- Fronteau, G., Moreau, C., Thomachot, C. and Barbin, V. (2010) Variability of some Lutetian building stones from the Paris Basin, from characterization to conservation. *Engineering Geology*, 115, 158–166.
- Jonscher, A.K. (1977) The 'universal' dielectric response. *Nature*, 267, 673–679.
- Keller, G.V. and Frischknecht, F.C. (1966) *Electrical Methods in Geophysical Prospecting*. Oxford: Pergamon Press.
- Kemna, A., Binley, A., Cassiani, G., Niederleithinger, E., Revil, A., Slater, L., *et al.* (2012) An overview of the spectral induced polarization method for near-surface applications. *Near Surface Geophysics*, 10, 453–468.
- Knight, R.J. and Nur, A. (1987) The dielectric constant of sandstones, 60 kHz to 4 MHz. *Geophysics*, 52–5, 644–654.
- Leroy, P. and Revil, A. (2009) A mechanistic model for the spectral induced polarization of clay minerals. *Journal of Geophysical Research*, 114, B10202.
- Loewer, M., Gunther, T., Igel, J., Kruschwitz, S., Martin, T. and Wagner, N. (2017) Ultra-broad-band electrical spectroscopy of soils and sediments – a combined permittivity and conductivity model. *Geophysical Journal International*, 210, 1360–1373.
- Niu, Q., Zhang, C. and Prasad, M. (2020) A framework for pore-scale simulation of effective electrical conductivity and permittivity of porous media in the frequency range from 1 MHz to 1 GHz. *Journal of Geophysical Research*, 125, e2020JB020515. <https://doi.org/10.1029/2020JB020515>
- Olhoeft, G.R. (1985). Low-frequency electrical properties. *Geophysics*, 50(12), 2492–2503.
- Rozenbaum, O., Le Trong, E., Rouet, J.L. and Bruand, A. (2007) 2D image analysis: a complementary tool for characterizing quarry and weathered building limestone. *Journal of Cultural Heritage*, 8, 151–159.
- Sass, O. and Viles, H.A. (2010) Wetting and drying of masonry walls: 2D resistivity monitoring of driving rain experiment on historic stonework in Oxford, UK. *Journal of Applied Geophysics*, 70, 72–83.
- Souffaché, B., Kessouri, P., Blanc, P. and Tabbagh, A. (2016) First investigations of in situ electrical properties of limestone blocks of ancient monuments. *Archaeometry*, 58(5), 705–721.
- Tabbagh, A., Cosenza, P., Ghorbani, A., Guérin, R. and Florsch, N., (2009) Modelling of Maxwell-Wagner induced polarization amplitude for clayey materials. *Journal of Applied geophysics*, 67(2), 109–113.

- Tabbagh, A., Rejiba, F., Finco, C., Schamper, C., Souffaché, B., Camerlynck, C., *et al.* (2021) The case for considering polarization in the interpretation of electrical and electromagnetic measurements in the 3 kHz to 3 MHz frequency range. *Surveys in Geophysics*, 42(2), 377–397. <https://doi.org/10.1007/s10712-020-09625-1>
- Topp, G.C., Davis, J.L. and Annan, A.P. (1980) Electromagnetic determination of soil water content: measurements in coaxial transmission lines. *Water Resources Research*, 16, 574–582.